Single-layer graphene on silicon nitride micromembrane resonators

Schmid, Silvan; Bagci, Tolga; Zeuthen, Emil; Taylor, Jacob M.; Herring, Patrick K.; Cassidy, Maja C.; Marcus, Charles M.; Villanueva Torrijo, Luis Guillermo; Armato, Bartolo; Boisen, Anja

Total number of authors:
15

Published in:
Journal of Applied Physics

Link to article, DOI:
10.1063/1.4862296

Publication date:
2014

Document Version
Publisher's PDF, also known as Version of record

Single-layer graphene on silicon nitride micromembrane resonators

Silvan Schmid, Tolga Bagci, Emil Zeuthen, Jacob M. Taylor, Patrick K. Herring, Maja C. Cassidy, Charles M. Marcus, Luis Guillermo Villanueva, Bartolo Amato, Anja Boisen, Yong Cheol Shin, Jing Kong, Anders S. Sørensen, Koji Usami, and Eugene S. Polzik

Citation: Journal of Applied Physics **115**, 054513 (2014); doi: 10.1063/1.4862296
View online: http://dx.doi.org/10.1063/1.4862296
View Table of Contents: http://scitation.aip.org/content/aip/journal/jap/115/5?ver=pdfcov
Published by the AIP Publishing

Single-layer graphene on silicon nitride micromembrane resonators

Silvan Schmid,[1] Tolga Bagci,[2] Emil Zeuthen,[2] Jacob M. Taylor,[3] Patrick K. Herring,[4] Maja C. Cassidy,[4] Charles M. Marcus,[5] Luis Guillermo Villanueva,[1] Bartolo Amato,[1] Anja Boisen,[1] Yong Cheol Shin,[6] Jing Kong,[6] Anders S. Sørensen,[2] Koji Usami,[2] and Eugene S. Polzik[2]

[1]*Department of Micro- and Nanotechnology, Technical University of Denmark, DTU Nanotech, Building 345 East, 2800 Kongens Lyngby, Denmark*
[2]*QUANTOP, Niels Bohr Institute, University of Copenhagen, 2100 Copenhagen, Denmark*
[3]*Joint Quantum Institute/NIST, College Park, Maryland 20899, USA*
[4]*School of Engineering and Applied Science, Harvard University, Cambridge, Massachusetts 02138, USA*
[5]*Center for Quantum Devices, Niels Bohr Institute, University of Copenhagen, 2100 Copenhagen, Denmark*
[6]*Department of Materials Science and Engineering, Massachusetts Institute of Technology, Cambridge, Massachusetts 02139, USA*

(Received 5 November 2013; accepted 31 December 2013; published online 7 February 2014)

Due to their low mass, high quality factor, and good optical properties, silicon nitride (SiN) micromembrane resonators are widely used in force and mass sensing applications, particularly in optomechanics. The metallization of such membranes would enable an electronic integration with the prospect for exciting new devices, such as optoelectromechanical transducers. Here, we add a single-layer graphene on SiN micromembranes and compare electromechanical coupling and mechanical properties to bare dielectric membranes and to membranes metallized with an aluminium layer. The electrostatic coupling of graphene covered membranes is found to be equal to a perfectly conductive membrane, without significantly adding mass, decreasing the superior mechanical quality factor or affecting the optical properties of pure SiN micromembranes. The concept of graphene-SiN resonators allows a broad range of new experiments both in applied physics and fundamental basic research, e.g., for the mechanical, electrical, or optical characterization of graphene. © *2014 AIP Publishing LLC*. [http://dx.doi.org/10.1063/1.4862296]

I. INTRODUCTION

Hybrid devices capable of coupling different systems are presently one of the hot topics in quantum technologies.[1,2] Recent proposals[3,4] outline optoelectromechanical systems, where a mechanical resonator is strongly coupled to an optical and an electrical resonator at the same time. The centerpiece of these proposals is a mechanical micromembrane inside an optical resonator which is capacitively coupled to an LC circuit.[3] Recently, such a hybrid optoelectromechanical system has been realized based on SiN-Al membranes.[5] For these applications, it is essential to have a strong electromechanical coupling relative to the mechanical properties of the membrane.

A key feature of SiN micromembranes is their ultrahigh quality factor (Q) reaching 10^6 to 10^7, low mass, and excellent optical transparency with losses less than 10^{-5} in the near infrared.[6–8] In order to not downgrade these essential properties, it was proposed to use dielectric polarization forces on bare SiN membranes for the electromechanical coupling.[3] Such forces on a dielectric are, however, inherently weaker than the forces on conductors. In this work, we deposit a single layer of graphene onto SiN membranes (SiN-G)[9] and compare their mechanical properties and electromechanical coupling to bare SiN membranes and to membranes covered with an aluminium layer (SiN-Al).[10] We show that this single layer of graphene allows superior electromechanical coupling without deteriorating the exceptional properties of SiN membranes. Importantly, our setup uses graphene in a floating electrode configuration. Thereby, graphene is not in contact with a metal and the interaction happens electrostatically. In this fashion, we avoid the large contact resistance associated with connecting graphene and a metal electrode.[11–13]

II. EXPERIMENTAL

We used commercial high and low-stress 50 nm thick Si_3N_4 membranes (Norcada, Inc.) for both the SiN and SiN-G resonators. Single layer graphene was grown on copper foil using standard CVD techniques.[14] The graphene on copper was cut to size, the copper wet-etched and the graphene (supported by a thin Poly(methyl methacrylate) (PMMA) film) transferred to the surface of the membrane in an aqueous environment. Once dry, the PMMA layer was removed from the graphene using acetone vapor. The characterization by Raman spectroscopy indicates that the single-layer graphene is of good quality.[15] The SiN-Al membranes were fabricated by standard cleanroom processing. The high-stress stoichiometric SiN layer is 100 nm thick. The aluminium layer is 50 nm thick and it is patterned by a lift-off step to create a round hole in the membrane center. A small rim (5% of the membrane size) along the anchor of the membrane was spared out in order to minimize damping.[10] Microscope images of the three membrane types are shown in Fig. 1(a).

Two types of coplanar electrode chips were used: interdigitated electrodes and quarter-segment electrodes.[16]

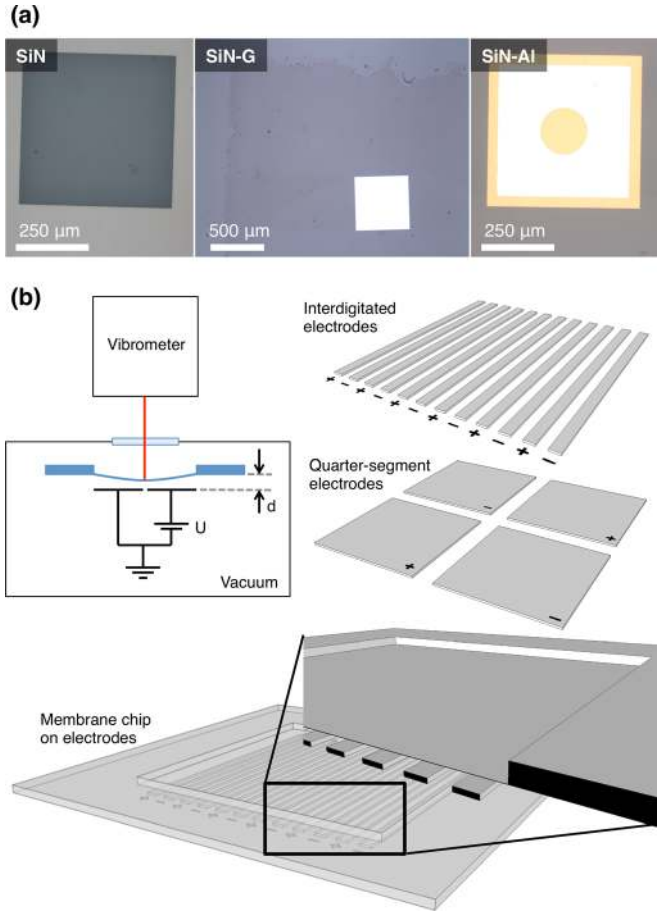

FIG. 1. (a) Microscope images of the three membrane types compared in this paper. (b) Schematic drawing of the experimental setup. The micromechanical membranes, with typical dimension of $0.5 \times 0.5\,\mathrm{mm}^2$ or $1 \times 1\,\mathrm{mm}^2$, are placed on top of coplanar electrodes. Two types of electrodes are used: interdigitated finger electrodes and quarter-segment electrodes.

Schematic drawings of the two types of electrodes are depicted in Fig. 1(b). The electrodes fabricated by standard cleanroom processing are made of a 200 nm thick gold layer sitting on borosilicate glass or SiN-covered silicon substrate. The chips are placed membrane downwards onto the electrode. The electrode chips feature pillars with a height of 600 nm and 1 μm in order to define a small gap between membrane and electrodes. Optical measurements of the gap distance d and the membrane vibrations have been made with a white light interferometer (vibrometer MSA-500 from Polytec GmbH, see disclaimer in Acknowledgments). The gap distance ranged from 3.5 μm to 14 μm which is larger than the height of the dedicated pillars. The larger measured distance can be ascribed to electrode chip unevenness coming from dirt and chip stress gradients.

The experimental setup is schematically depicted in Fig. 1. The membrane-electrode sandwich is placed in a vacuum chamber (pressure below 1×10^{-5} millibars) and is electrically connected to an external voltage source. For quality factor measurements, the membranes were placed on a piezo for stimulation. Q was extracted from the ring-down time or the -3 dB bandwidth of the resonance peak.

III. ELECTROMECHANICAL MODEL

In the case where the electrostatic coupling is symmetric with respect to the two electrode polarities and neglecting the effect of free charges on the membrane, the electrostatic force between a dielectric or conductive thin membrane and electrodes can generally be described by

$$F = cAf(d)U^2, \tag{1}$$

with the area of the segment A, distance between fixed electrodes and membrane d, DC voltage U between fixed electrodes, and an electrostatic force constant c; $f(d)$ is a scaling function with units of inverse area.

The equilibrium of forces for an infinitesimal piece of membrane with the area $dx \times dy$ and thickness h is

$$\sigma_0 h \nabla^2 w(x,y,t) - \rho h \frac{\partial^2 w}{\partial t^2}(x,y,t) + cU^2 f(d - v(x,y,t))\xi(x,y) = 0, \tag{2}$$

with the displacement function $v(x, y, t)$, the tensile prestress σ_0, and the mass density ρ. $\xi(x, y)$ is a Heaviside step function (or a product of such functions) taking into account electrode gaps and edges, as well as the hole in the membrane metallization of some of the membranes used.

The deflection of a membrane can be described by

$$v(x,y,t) = \sum_{n=1}^{\infty}\sum_{m=1}^{\infty} A_{nm}\Phi_{n,m}(x,y)\, e^{i\omega t}, \tag{3}$$

with the mode shape function

$$\Phi_{n,m}(x,y) = \sin\frac{n\pi x}{L_x}\sin\frac{m\pi y}{L_y}. \tag{4}$$

Considering the first order Taylor approximation of the electrostatic force (1), the equation of motion can be written as

$$\sigma_0 h \nabla^2 v - \rho h \frac{\partial^2 v}{\partial t^2} + \left(cU^2 f(d) - cU^2 f'(d) v\right)\xi(x,y) = 0. \tag{5}$$

In a "linear system," the static force term $cU^2 f(d)\xi(x,y)$ causes a static deflection of the membrane. This static deflection does not influence the eigenfrequency and can thus be neglected. Following Galerkin's method, (2) can be solved for the fundamental normal mode by multiplying it with $\Phi_{1,1}$ and integrating over the entire membrane area $A = L \times L$ with $L = L_x = L_y$

$$\iint_A \left(\sigma_0 h \nabla^2 v + \rho h \omega^2 v - cU^2 f'(d) w \xi(x,y)\right)\Phi_{1,1}\,\mathrm{d}x\,\mathrm{d}y = 0, \tag{6}$$

which with (3) can be written as

$$-2\frac{\pi^2}{L^2}\sigma_0 h \iint_A \Phi_{1,1}^2\,\mathrm{d}x\,\mathrm{d}y + \rho h \omega^2 \iint_A \Phi_{1,1}^2\,\mathrm{d}x\,\mathrm{d}y - cU^2 f'(d)\iint_A \Phi_{1,1}^2\,\xi(x,y)\,\mathrm{d}x\,\mathrm{d}y = 0, \tag{7}$$

where we have ignored the induced couplings to other membrane modes assumed to be weak.

The frequency can now be isolated from (7)

$$\omega^2 = 2\pi^2 \frac{\sigma_0}{\rho}\frac{1}{L^2} + c\frac{U^2 f'(d)}{h\rho}\frac{\int\int_A \Phi_{1,1}^2 \xi(x,y)\mathrm{d}x\,\mathrm{d}y}{\int\int_A \Phi_{1,1}^2 \mathrm{d}x\,\mathrm{d}y}. \quad (8)$$

With the eigenfrequency ω_0 of a membrane with zero voltage applied ($U=0$)

$$\omega_0 = \frac{\sqrt{2}\pi}{L}\sqrt{\frac{\sigma_0}{\rho}}, \quad (9)$$

and introducing the overlap factor $\eta_{1,1}$ between the membrane mode $\Phi_{1,1}$ and the electrode mask

$$\eta_{1,1} = \frac{\int\int_A \Phi_{1,1}^2 \xi(x,y)\mathrm{d}x\,\mathrm{d}y}{\int\int_A \Phi_{1,1}^2 \mathrm{d}x\,\mathrm{d}y}, \quad (10)$$

the first order Taylor approximation of ω becomes

$$\omega \approx \omega_0\left(1 + c\frac{U^2 f'(d)}{2h\rho\omega_0^2}\eta_{1,1}\right), \quad (11)$$

which results in a relative frequency shift of

$$\frac{\Delta\omega}{\omega_0} = \frac{U^2 f'(d)}{2h\rho\omega_0^2}\eta_{1,1}. \quad (12)$$

For a membrane with a continuous electrode ($\xi = 1 \Rightarrow \eta_{1,1} = 1$), the frequency shift due to the electrostatic spring softening effect becomes

$$\frac{\Delta\omega}{\omega_0} = c\frac{U^2 f'(d)}{2h\rho\omega_0^2}. \quad (13)$$

IV. RESULTS AND DISCUSSION

A. Quality factor

A key feature of micromechanical membranes is their Q of up to several million. Such high Qs are a requirement for strong optomechanical coupling and for high resolution measurements. It has been shown that a metal coating increases the energy loss in a membrane which results in a reduction of Q. The contribution of the mechanical dissipation of the metal layer can be minimized by leaving the membrane area close to the clamping, where the maximal mechanical strain occurs, uncoated.[10,17] In the first experiment, we compared the quality factors of the 3 different types of membranes. Fig. 2 shows the measured Qs of a bare SiN, SiN-Al, and SiN-G membrane. On the SiN-Al membrane a rim of 5% of the membrane dimension remained uncoated, whereas graphene is fully covering the entire SiN-G membrane. The quality factors are highly mode dependent and the measured values are in correspondence with values measured by Yu *et al.*[10] There are clearly two sets of Q-values. According to Ref. 10, the lower set (below ~100 000) is limited by clamping losses. The higher set is limited by intrinsic damping, such as bulk or surface losses. It can be seen from the measurements that there is no significant difference between the different membrane types. The graphene seems to be mechanically invisible and it does not significantly contribute to the energy loss. Thus, with graphene it is not required to spare out the membrane area close to the clamping edge as it is for the Al layer. A similar finding, that the damping contribution of the additional graphene layer is small compared to an additional metal layer, has been made by Lee *et al.*[9]

B. Electrostatic coupling

It is crucial for an efficient hybrid optoelectromechanical device to have strong electromechanical coupling between the membrane and the electrical circuit. The electrostatic interaction for SiN membranes is due to dielectric polarization forces (the electric field interacts with a dielectric)[3,18–20] and in some of the experiments presented here it is also due to the quasi-permanent electric charges in a dielectric. The interdigitated electrodes have been design to generate strong electric field gradients required for the dielectric polarization force. The interaction for conductive SiN-Al[1] is due to the electrostatic force between conductors (the electric field interacts with charges on a conductor). For this case, the quarter-segment electrodes have been designed.[21] Using the two electrode geometries allow us to characterize the comparative performance of both types of membranes. It also allows us to conclude to which type the SiN-G membranes belong.

We extract the intrinsic coupling strength c of each membrane type from measuring the mechanical frequency shift due to the so-called spring softening effect which, according to (12), results in a quadratic frequency drop with the DC-bias voltage U_{DC}

$$\frac{\Delta\omega}{\omega_0} = -\alpha U_{DC}^2. \quad (14)$$

Using α found from the frequency shift data, the electrostatic force constant c can then be calculated

$$c = 2\alpha[-f'(d)]^{-1}h\rho\omega_0^2\eta^{-1}. \quad (15)$$

Here, the coupling performance of SiN-G membranes is compared to that of the SiN and SiN-Al membranes using the two types of capacitor + membrane chips described above. In the first set, SiN and SiN-G membranes are coupled to interdigitated electrodes; in the second set, SiN-Al and SiN-G membranes are coupled to quarter-segment electrodes.

1. Interdigitated electrodes

For the interdigitated electrode geometry and the range of membrane-capacitor distances d used in the experiments,

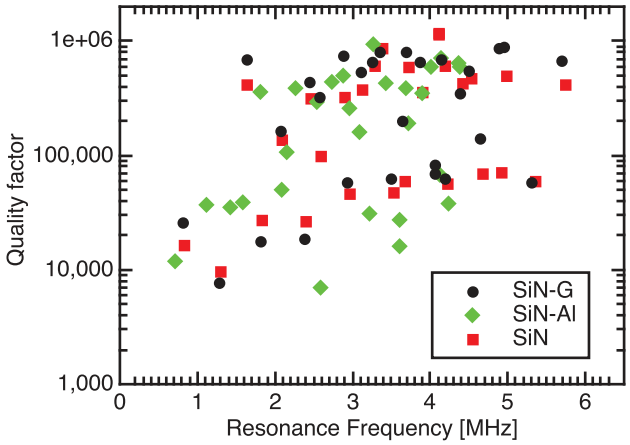

FIG. 2. Quality factors versus resonance frequency of higher modes of a SiN-G membrane compared to a bare SiN and a SiN-Al membrane. The membranes have a diameter of $0.5 \times 0.5\,\mathrm{mm}^2$ and are all made of high-stress stoichiometric SiN.

the electrostatic force for both dielectric and perfectly conducting membranes (an appropriate model for our SiN-G membranes) is well approximated by

$$f(d) = A_0^{-1} e^{-\kappa d}, \tag{16}$$

with A_0 as a scaling constant with units of area. For the data presented below, we use $A_0 = 1\,\mu\mathrm{m}^2$. For our specific setup, we determined numerically that $\kappa = 1.05\,\mu\mathrm{m}^{-1}$ for both dielectric and perfectly conducting membranes.

In Fig. 3(a), the electrostatic spring softening of a SiN-G membrane on top of an interdigitated electrode is shown. From the fit parameter α obtained from this data, the force constant c is calculated for the membranes using Eq. (15) and the exponential force law (16). The resulting average force constants for the bare SiN and SiN-G membranes on interdigitated electrodes are shown in the left part of Fig. 3(c). SiN-G is seen to outperform SiN by a factor of 5.5. Also shown are the theoretical values determined semi-analytically for dielectric (SiN, $\varepsilon_r = 7.6$) and perfectly conducting membranes; the average force constant of SiN-G is seen to be compatible with the latter.

2. Quarter-segment electrodes

Next, we use the quarter-segment coplanar electrodes with a SiN-Al or a SiN-G membrane as a floating electrode. The results of this set of experiments are well described by another force law (in the regime where d is smaller than the inter-electrode gap)

$$f(d) = \frac{1}{d^2}. \tag{17}$$

The measured spring softening of a SiN-G membrane placed over quarter segment electrodes is shown in Fig. 3(b). From the fit parameter α obtained from this data, the force constant c is calculated for the conducting membranes again with Eq. (15) but now using the quadratic force law (17). On the right side of Fig. 3(c), the extracted average force constants of SiN-G and SiN-Al membranes are shown. The

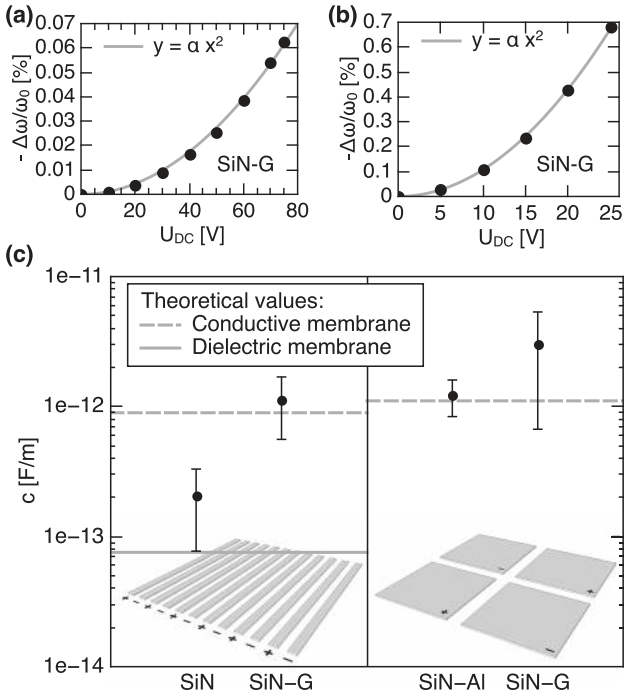

FIG. 3. Extraction and comparison of the electrostatic force constant c. Spring softening of (a) a SiN-G membrane ($0.5 \times 0.5\,\mathrm{mm}^2$, $d = 7.0\,\mu\mathrm{m}$) on interdigitated electrodes and (b) a SiN-G membrane ($0.5 \times 0.5\,\mathrm{mm}^2$, $d = 6.3\,\mu\mathrm{m}$) to quarter-segment electrodes. (c) Comparison of force constants c (according to (15) using (16) and (17)) for different combinations of electrodes and membranes. On the left, c extracted for bare SiN (4 experiments) and SiN-G (3 experiments) membranes on interdigitated electrodes are shown. The electrode fingers are $4\,\mu\mathrm{m}$ wide with a gap of $2\,\mu\mathrm{m}$ between the fingers. To the right, c of SiN-Al (3 experiments) and SiN-G (4 experiments) on quarter-segment electrodes are shown. The error bars represent the standard deviation. The solid and dashed grey lines represent the theoretical values for the scenario of a pure dielectric polarization force and an electrostatic force on the conductive membrane, respectively.

experimental values again agree well with the theoretical value for a perfect conductor of $c = \frac{1}{8}\varepsilon_0$.[15] The large standard deviation of the force constant can be assigned to uncertainties in the distance d measurement and lateral misalignment which can contribute up to 20% error. The relatively large average c value of the SiN-G membranes might be an effect due to the excess graphene on the frame.[15]

3. Charging

An additional complication with SiN membranes which is eliminated by using SiN-Al or SiN-G membranes is the accumulation of free charges on the dielectric SiN membrane. The charging has been investigated by increasing the DC voltage and then inverting the polarity. If quasi-static charges are present, a spring hardening (increase in oscillation frequency) instead of softening will be observed. The results of this experiment are shown in Fig. 4 with a bare SiN, a SiN-Al, and a SiN-G membrane on interdigitated electrodes. From the observed spring hardening, shown in Fig. 4(a), it can be concluded that free electric charges are indeed available on the bare SiN membranes. We note that the force on a charge is a function of the inverse of the distance ($\propto 1/d$) and may therefore be partly responsible for the somewhat higher value of

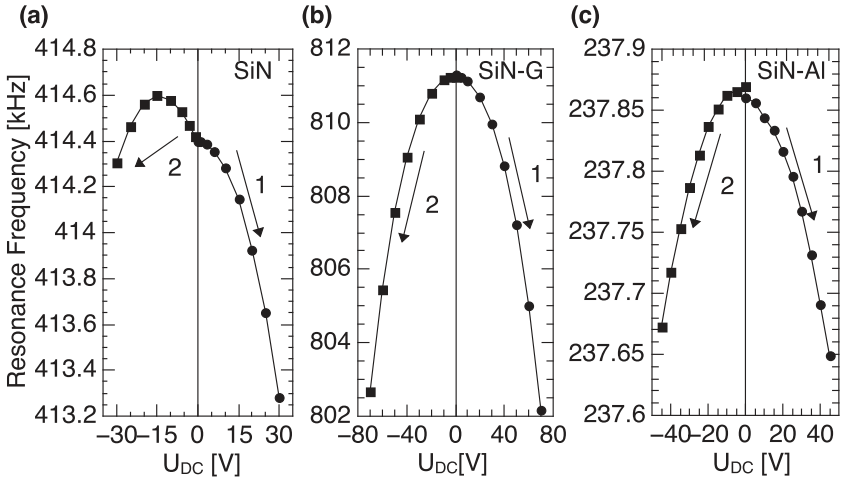

FIG. 4. Response of the resonance frequency of fundamental mode of a bare SiN, a SiN-G, and a SiN-Al membrane to DC polarity inversion. First, the voltage was increased in the positive direction. Then, the polarity was reversed and the voltage was increased in the negative direction. (a) Response of a bare SiN membrane ($1 \times 1\,\text{mm}^2$, $d = 4.0\,\mu\text{m}$) on interdigitated electrodes; electrode fingers are $4\,\mu\text{m}$ wide with a gap of $2\,\mu\text{m}$ between the fingers. (b) Response of a SiN-G membrane ($0.5 \times 0.5\,\text{mm}^2$, $d = 5.5\,\mu\text{m}$) on interdigitated electrodes; the electrode fingers are $4\,\mu\text{m}$ wide with a gap of $5\,\mu\text{m}$ between the fingers. (c) Response of a SiN-Al membrane ($1 \times 1\,\text{mm}^2$, $d = 11\,\mu\text{m}$) on quarter-segment electrodes. The resonance frequency was determined from the thermomechanical resonance peak.

the coupling constant c for SiN shown in Fig. 3(c). The details of the experiment in Fig. 4(a) including the charging related hysteresis are given in the supplementary material.[15]

Figs. 4(b) and 4(c) present the results of the same charging experiment conducted with a SiN-G on similar interdigitated electrodes and with SiN-Al membranes on quarter-segment electrodes, respectively. Assuming that the electrode design does not influence the charging effect, we conclude that the absence of spring hardening for SiN-G shows that the single layer of graphene as well as the Al layer eliminates charging. This is supported by the pure electrostatic behavior of the SiN-G membranes as shown in Fig. 5. If the AC driving voltage is small compared to the DC bias voltage, the electrostatic force becomes

$$F = cAf(d)(U_{DC} + U_{AC})^2 \approx cAf(d)(U_{DC}^2 + 2U_{AC}U_{DC}). \quad (18)$$

Thus, the mechanical resonance peak amplitude is approximately a linear function of the DC voltage (Fig. 5(a)), for a fixed AC driving voltage, and the static deflection of the membrane is a quadratic function of the DC voltage (Fig. 5(b)).

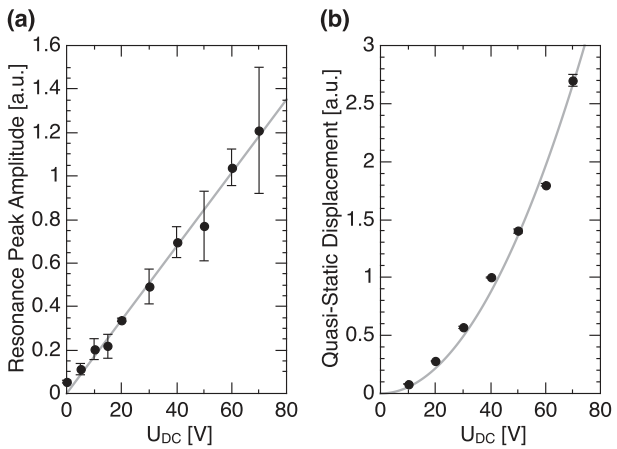

FIG. 5. Response of fundamental mode of a $0.5 \times 0.5\,\text{mm}^2$ SiN-G membrane on interdigitated electrodes. Response of (a) resonance peak amplitude and (b) quasi-static displacement to DC bias voltage. The distance between membrane and electrodes is $d = 6.5\,\mu\text{m}$. The electrode fingers are $4\,\mu\text{m}$ wide with a gap of $5\,\mu\text{m}$ between the fingers. The resonance peak amplitude was measured for a white noise signal of $U_{AC} = 10\,\text{mV}$. The quasi-static displacement was measured with a rectangular signal at 10 kHz (which is far below the fundamental resonance frequency and can therefore be considered to be quasi-static). The error bars represent the standard deviation of 3 consecutive measurements. The grey lines represent a linear fit in (a) and a quadratic fit in (b).

V. CONCLUSION

In conclusion, we have shown that SiN-G membranes with a single layer of graphene are promising candidates for efficient optoelectromechanical resonators. Furthermore, by using graphene on SiN in a floating electrode configuration, we overcome the unsolved problem of high contact resistance between metal electrodes and graphene. They show electromechanical coupling which is as good as for an ideal conductor. The enhanced electromechanical coupling of conductive membranes lowers the threshold for strong coupling, as predicted for dielectric membranes,[3] accordingly. The single graphene layer is mechanically invisible and does not negatively influence the membrane performance. Unlike the real metal coating, graphene does not require patterning in order to maintain the highest mechanical quality factors of a bare SiN membrane. Also, unlike the metal coating, graphene does not add any noticeable mass to the membrane which is an advantage for high sensitivity applications, such as, e.g., the optical detection of radio waves with metallized silicon nitride membrane resonators.[5] The lower mass achieved by SiN-G membranes as compared to SiN-Al membranes used in the reference would improve the quantum efficiency of radio frequency (RF)-to-optical conversion by up to 4 times (by the ratio of the masses). Finally, the use of

graphene overcomes the complications of charging effects in SiN membranes, which has shown to be difficult to control.

ACKNOWLEDGMENTS

We acknowledge funding from the DARPA program QUASAR, the EU projects QESSENCE and NANODEVICE, the ERC projects INTERFACE and QIOS (Grant Agreement No. 306576), and the Villum Kann Rasmussen Centre of Excellence "NAMEC" under Contract No. 65286. We would like to thank Louise Jørgensen for cleanroom support and Martin Benjamin B. S. Larsen for support with the Raman measurements. Certain commercial equipment, instruments or materials are identified in this paper to foster understanding. Such identification does not imply recommendation or endorsement by the National Institute of Standards and Technology, nor does it imply that the materials or equipment are necessarily the best available for the purpose.

[1]J. D. Teufel, D. Li, M. S. Allman, K. Cicak, A. J. Sirois, J. D. Whittaker, and R. W. Simmonds, Nature **471**, 204 (2011).
[2]E. Gavartin, P. Verlot, and T. J. Kippenberg, Nat. Nanotechnol. **7**, 509 (2012).
[3]J. M. Taylor, A. S. Sørensen, C. M. Marcus, and E. S. Polzik, Phys. Rev. Lett. **107**, 273601 (2011).
[4]C. A. Regal and K. W. Lehnert, J. Phys. Conf. Ser. **264**, 012025 (2011).
[5]T. Bagci, A. Simonsen, S. Schmid, L. G. Villanueva, E. Zeuthen, J. Appel, J. M. Taylor, A. Sørensen, K. Usami, A. Schliesser, and E. S. Polzik, "Optical detection of radio waves through a nanomechanical transducer," preprint arXiv:1307.3467 [physics.optics] (2013).
[6]J. D. Thompson, B. M. Zwickl, A. M. Jayich, F. Marquardt, S. M. Girvin, and J. G. E. Harris, Nature **452**, 72 (2008).
[7]D. J. Wilson, C. A. Regal, S. B. Papp, and H. J. Kimble, Phys. Rev. Lett. **103**, 207204 (2009).
[8]T. J. Kippenberg and K. J. Vahala, Opt. Express **15**, 17172 (2007).
[9]S. Lee, V. P. Adiga, R. A. Barton, A. van der Zande, G.-H. Lee, B. R. Ilic, A. Gondarenko, J. M. Parpia, H. G. Craighead, and J. Hone, Nano Lett. **13**, 4275 (2013).
[10]P.-L. Yu, T. P. Purdy, and C. A. Regal, Phys. Rev. Lett. **108**, 083603 (2012).
[11]S. Russo, M. F. Craciun, M. Yamamoto, A. F. Morpurgo, and S. Tarucha, Physica E **42**, 677 (2010).
[12]A. Venugopal, L. Colombo, and E. M. Vogel, Appl. Phys. Lett. **96**, 013512 (2010).
[13]K. S. Novoselov, V. I. Fal'ko, L. Colombo, P. R. Gellert, M. G. Schwab, and K. Kim, Nature **490**, 192 (2012).
[14]X. Li, W. Cai, J. An, S. Kim, J. Nah, D. Yang, R. Piner, A. Velamakanni, I. Jung, E. Tutuc, S. K. Banerjee, L. Colombo, and R. S. Ruoff, Science **324**, 1312 (2009).
[15]See supplementary material at http://dx.doi.org/10.1063/1.4862296 for graphene Raman spectra; theoretical value calculation of force constant; and discussion of effect of excess graphene and charging related hysteresis measurements.
[16]J. U. Jeon and T. Higuchi, IEEE Trans. Ind. Electron. **45**, 938 (1998).
[17]S. Schmid, K. D. Jensen, K. H. Nielsen, and A. Boisen, Phys. Rev. B **84**, 165307 (2011).
[18]S. Schmid, M. Wendlandt, D. Junker, and C. Hierold, Appl. Phys. Lett. **89**, 163506 (2006).
[19]S. Schmid, C. Hierold, and A. Boisen, J. Appl. Phys. **107**, 054510 (2010).
[20]Q. P. Unterreithmeier, E. M. Weig, and J. P. Kotthaus, Nature **458**, 1001 (2009).
[21]S. Kumar, D. Cho, and W. N. Carr, J. Microelectromech. Syst. **1**, 23 (1992).